Metamaterial-based microfluidic sensor for dielectric characterization

Withawat Withayachumnankul,[1,a] Kata Jaruwongrungsee,[b,c]
Adisorn Tuantranont,[c] Christophe Fumeaux,[a] and Derek Abbott[a]

[a]*School of Electrical & Electronic Engineering, The University of Adelaide, Adelaide, SA 5005*

[b]*School of Electronic Engineering, Faculty of Engineering,*
King Mongkut's Institute of Technology Ladkrabang, Bangkok 10520, Thailand

[c]*Nanoelectronics and MEMS Laboratory,*
National Electronics and Computer Technology Center, Pathumthani 12120, Thailand

Abstract

A microfluidic sensor is implemented from a single split-ring resonator (SRR), a fundamental building block of electromagnetic metamaterials. At resonance, an SRR establishes an intense electric field confined within a deeply subwavelength region. Liquid flowing in a micro-channel laid on this region can alter the local field distribution and hence affect the SRR resonance behavior. Specifically, the resonance frequency and bandwidth are influenced by the complex dielectric permittivity of the liquid sample. The empirical relation between the sensor resonance and the sample permittivity can be established, and from this relation, the complex permittivity of liquid samples can be estimated. The technique is capable of sensing liquid flowing in the channel with a cross-sectional area as small as $(0.001\lambda_0)^2$, where λ_0 denotes the free-space wavelength of the wave excitation. This work motivates the use of SRR-based microfluidic sensors for identification, classification, and characterization of chemical and biochemical analytes.

Keywords: metamaterial; split-ring resonator; microfluidic sensing; dielectric characterization

1. Introduction

Recently, an alternative sensing platform based on electromagnetic metamaterials has been introduced. Electromagnetic metamaterials belong to the class of artificially engineered materials. They are made of subwavelength resonators that collectively respond to an incident wave. Owing to the subwavelength size of these resonators, the cluster can be regarded as being a homogeneous material providing an effective electromagnetic response [1]. As a main component, the resonator is typically realized using a metallic open loop with a dielectric gap to sustain a strong resonance. Depending on their geometry and orientation, the inclusions can couple with free-space electric or magnetic waves at a wavelength much longer than the periodicity. At resonance, they develop a strong current oscillation in the metallic loop and a localised electric field in the gap. This local resonant field is very sensitive to a change in the dielectric contained in the subwavelength gap region. The high sensitivity of metamaterial resonators to a small amount of dielectric material is promising for sensing applications.

The benefit of metamaterials leads to implementation for material sensing in different spectral ranges, from microwaves, terahertz, infrared, to optics. Substances under test include solid dielectrics [2,3,4], liquids [5,6], and biomolecules [7,8,9], developed in the form of solid or liquid films. Most of the studies have merely investigated the function of metamaterial resonators for detecting the presence and/or estimating the amount of the sample. A particular finding has shown that it is possible to determine the refractive index and thickness of dielectrics under test from the resonance shift [6]. None of these earlier studies have characterized the sample complex electric permittivity, despite the fact that the exhibited resonance contains complete information on the dielectric constant and loss tangent of the sample.

A few recent studies on metamaterials involved microfluidic applications [10,11,12]. These particular cases employed microfluidic channels to tune the resonance frequency or to deliver the liquid or dissolved analyte into the sensing area. In Refs [10,11], a planar metamaterials was fitted with a group of liquid tubes, each

[1] Corresponding author at: School of Electrical and Electronic Engineering, The University of Adelaide, Adelaide, SA 5005. Tel. +61 8 8313 1812: fax: +61 8 8313 4360. E-mail address: withawat@eleceng.adelaide.edu.au.

running along a row of resonators. It was shown that loading static liquid into the tubes caused a significant shift in the resonance. Notably, this planar configuration required a relatively large volume of liquid to cover the entire resonator array. Further to this, a left-handed microstrip transmission line composed of multiple spiral resonators was assembled with an S-shaped microfluidic channel to sense liquid mixtures [12]. This particular design results in a bandpass response due to resonance broadening, and a relatively large sensing area owing to the distributed capacitance of the spiral resonators. The implication is degradation in the robustness and sensitivity of the sensor. It is obvious that none of these microfluidic configurations fully leveraged the capability of metamaterials, i.e., field localization and high Q resonance, for microfluidic sensing. In addition, these relevant studies do not suggest an approach to determining the complex permittivity of the sample.

This article presents a microfluidic sensor based on a high-Q metamaterial resonator. The sensor mainly comprises a single SRR, proximity-coupled to a microstrip transmission line. A microfluidic channel is aligned across the deeply subwavelength localized gap region of the SRR for maximum exposure of the flowing liquid to the confined electric field. The information obtained from the sensor is used to determine the sample complex permittivity, which is applicable to concentration analysis and substance identification/classification. Since the liquid is directly probed by the electric field, the system is label-free, real-time, and nondestructive. The sensing module is either disposable or reusable. Note that a similar system of dual SRRs excited by a coplanar waveguide has recently been mentioned briefly in a review article, however, with no further analysis or experimental verification [13].

2. Principle

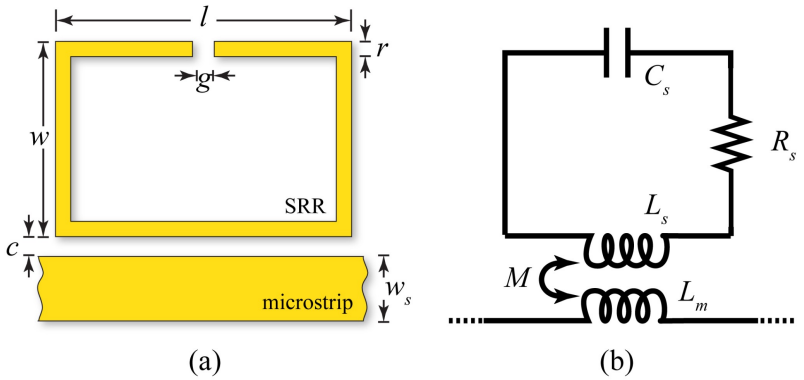

Figure 1. Microstrip-coupled SRR. (a) Diagram (not to scale) of the SRR and microstrip with dimensions as follows: l = 7 mm, w = 7.5 mm, g = 0.15 mm, r = 0.2 mm, c = 0.65 mm, and w_s = 1.7 mm. The metallic structure is supported by a dielectric substrate, which also supports the ground plane on its bottom side. (b) Equivalent circuit with L_m for the inductance of the microstrip line, $\{RLC\}_S$ for the parasitic elements of the ring, and M for the mutual inductance between the ring and line.

Figure 1(a) depicts the diagram of a microstrip-coupled SRR, representing a main component of the proposed microfluidic sensor. The SRR is made of metal loop with a square shape and a split on one side. The microwave launched into an end of the microstrip line excites the quasi-TEM mode of wave propagation. This mode is described by an oscillating current along the strip and a magnetic field circulating around the strip. The magnetic field can induce current in the nearby SRR when the magnetic component is in parallel to the SRR axis. The resonance occurs when the electric energy stored in the SRR gap is equal to the magnetic energy stored in the SRR loop. As illustrated in the inset of Fig 2, on resonance a strong electric field is established across the dielectric gap. This resonance is observable in the microstrip transmission curve as shown in Fig. 2. Note that as an alternative, a free-space wave excitation can be used instead of this microstrip line coupling, but hundreds of SRRs and a large amount of sample are required to yield an observable resonance effect.

In the quasi-static limit, the system of a SRR and transmission line can be approximated by fundamental circuit elements, as shown in Fig. 1(b). The SRR loop is responsible for the inductance L_S and the gap for the capacitance C_S. Effectively, the SRR forms a series RLC resonant circuit. By omitting the effect of the mutual inductance M, the impedance of the resonator can be described as

$$Z_s = R_s + j\omega L_s + \frac{1}{j\omega C_s} \quad (1)$$

The capacitance C_s is affected by the dielectric materials around the gap, and can be roughly approximated by

$$C_s = C_0 + \epsilon_{sam} C_c \quad (2)$$

where C_0 includes the capacitive effect from the dielectric substrate, channel walls, and surrounding space, excluding the channel cavity. The term $\varepsilon_{sam} C_c$ describes the contribution from the loaded liquid sample with C_c for the capacitance of an empty channel and $\varepsilon_{sam} = \varepsilon'_{sam} + j\varepsilon''_{sam}$ for the complex permittivity of the sample. It is assumed that the fringing field pattern does not change with sample loading. By substituting Eq. (2) into Eq. (1), it can be shown that the total resistance R_t and capacitance C_t of the SRR are a function of the sample permittivity, or

$$R_t = F_R(\epsilon'_{sam}, \epsilon''_{sam}) \text{ and } C_t = F_C(\epsilon'_{sam}, \epsilon''_{sam}) \quad (3)$$

Both R_t and C_t are the factors that determine the resonance characteristics, i.e., the resonance frequency,

$$f_0 = \frac{1}{2\pi\sqrt{L_s C_t}} \quad (4)$$

and Q factor,

$$Q = \frac{1}{R_t}\sqrt{\frac{L_s}{C_t}} \quad (5)$$

Therefore, from Eqs. (3-5), it is clear that the SRR resonance is dominated by the complex permittivity of the sample. By analyzing this dependency, it is possible to retrieve the dielectric characteristics of the liquid sample from the measurable transmission resonance.

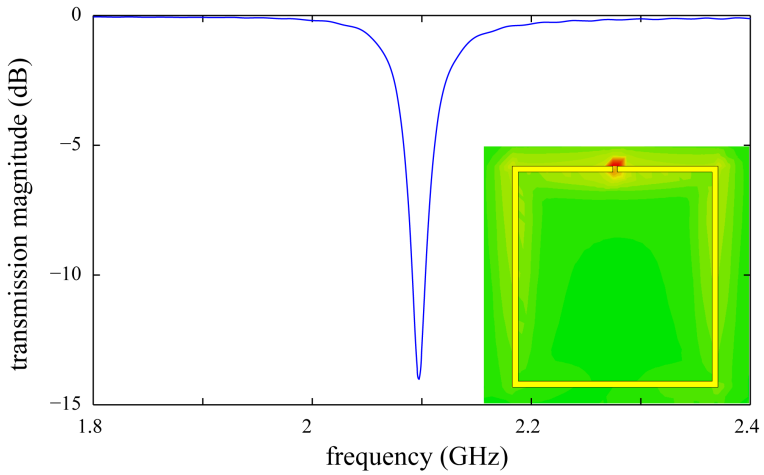

Figure 2. Numerically resolved transmission magnitude of the SRR-loaded microstrip. (Inset) Absolute electric field strength over the surface of the structure at 2.1 GHz. The results are for the structure in Fig. 1(a), and are determined with a commercial full-wave electromagnetic solver, CST Microwave Studio, based on the Finite-Integration Technique (FIT).

3. Fabrication and measurement

The SRR-based sensor shown in Fig 3(a) is fabricated by using standard photolithography and chemical etching with the dimensions given in Fig 1(a). The 50-Ω microstrip line, SRR, and ground plane are made from gold-coated copper with the copper thickness of 35 μm. The substrate is an RT/duroid 6010.2LM high-frequency laminate (ceramic-PTFE composite) with a thickness of 1.90 mm, a relative permittivity of 10.2, and a loss tangent of 0.0023. The microfluidic flow-channel is made by craft-cutting a PET film with a

channel height, width, and length of 60 μm, 0.6 mm, and 3.0 mm, respectively. The channel is mechanically pressed against the substrate with waterproof adhesive filling the gap between them. As shown in Fig 3(b), the channel is manually positioned across the SRR gap so that the liquid sample can flow straight into the sensing area. This well-defined channel ensures the consistency of the volume and shape of the analyte over the gap area. Note that the resonance is partly influenced by the exact position of the microfluidic channel. However, this is not an issue since the measurement is relative, and the channel position does not change during measurement. Figure 3(c) shows the fully assembled sensor module that is connected to the polymer tubes and coaxial cables.

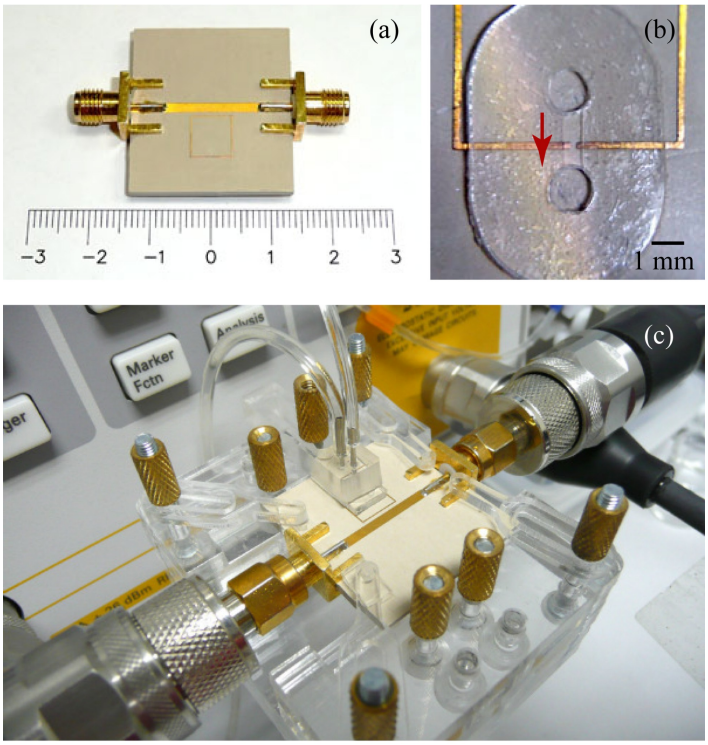

Figure 3. Assembled sensor module. (a) Fabricated microstrip-coupled SRR with two SMA connectors. The scale is in cm. (b) A zoom-in showing the microfuidic chamber attached to the SRR. The channel with inlet/outlet is laid onto the SRR gap. The arrow indicates the flow direction. (c) Fully assembled module with polymer tubes delivering liquid into the chamber and coaxial cables connected to the vector network analyzer.

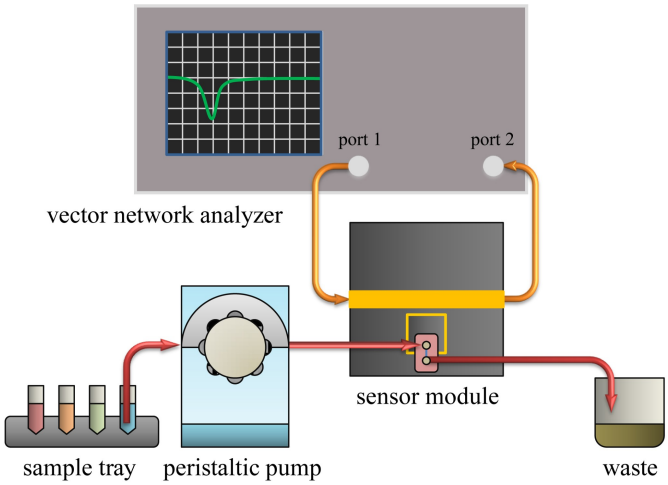

Figure 4. Diagram of the experimental setup. The equipment is mainly composed of the vector network analyzer, peristaltic pump, and sensor module. All measurements are performed at room temperature, i.e., around 25 ºC.

The experimental setup is outlined in Fig. 4. During measurement, the response of the sensor is monitored in real time with the vector network analyzer that can sweep across the microwave frequency range of interest. The *stop-flow* technique is employed, i.e., the peristaltic pump fills the liquid sample into the microfluidic channel and then the flow is stopped for measurement. Any change in the liquid permittivity

causes a change in the transmission resonance. It has been experimentally verified that the continuous flow does not affect the measurement results, as long as the pressure is low enough to avoid channel deformation. Examples of the transmission response of the sensor module are given in Fig. 5. The resonance frequency and Q factor are highest when the SRR is left fully exposed to the free space without liquid chamber above the gap. As the empty chamber is installed, a part of the sensitive gap area is covered, resulting in a slightly lower resonance frequency and Q factor. Depending on their complex permittivity, different samples filling the channel change the resonance characteristics differently, as visible in the figure for the cases of ethanol and water. From the results, it is clear that the liquid analyte with a cross sectional area as small as $(0.001\lambda_0)^2$ can induce a large change in the resonance. Different resonance responses of the sensor will be further analyzed in Section 4.

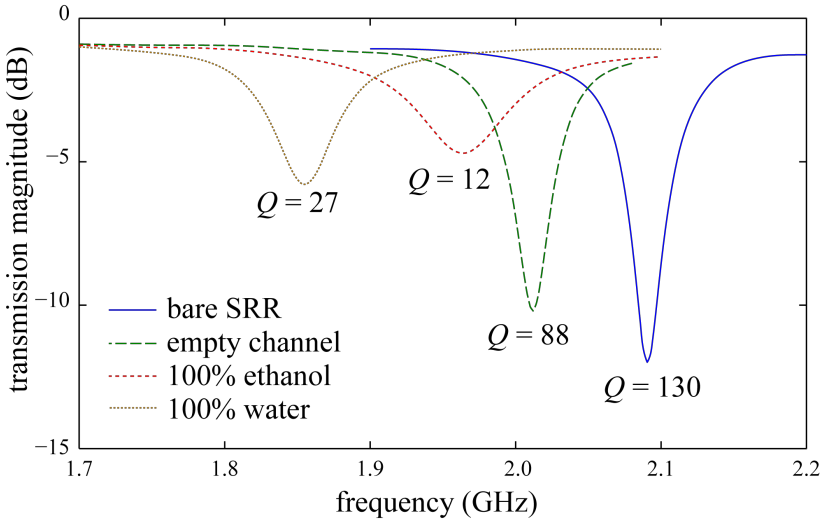

Figure 5. Measured transmission response of the sensor module. The profiles represent different measurement conditions: the bare SRR structure without the microfluidic chamber, the assembled sensor with an empty channel, the sensor with channel filled with 100% ethanol, and with 100% water. The Q factor is defined as $f_0/\Delta f$, where Δf is the bandwidth at +3 dB with respect to the minimal transmission.

4. Sensor's characteristics

As shown in Section 2, the resonance frequency and Q factor are related to the complex permittivity of the sample through nonlinear functions. The relation is further complicated by the complex geometry around the sensing area. In order to simplify the problem, a set of linear functions can be used to approximate the interdependency. In this case, an assumption is made that variations in the real and imaginary parts of the permittivity are small enough around a given reference. The simplified model that relates changes in the permittivity to variations in the resonance frequency and Q factor can be expressed in the matrix form as

$$\begin{bmatrix} \Delta f_0 \\ \Delta Q \end{bmatrix} = \begin{bmatrix} m_{11} & m_{12} \\ m_{21} & m_{22} \end{bmatrix} \begin{bmatrix} \Delta \epsilon' \\ \Delta \epsilon'' \end{bmatrix}, \tag{6}$$

where $\Delta\varepsilon' = \varepsilon'_{sam} - \varepsilon'_{ref}$, $\Delta\varepsilon'' = \varepsilon''_{sam} - \varepsilon''_{ref}$, $\Delta f_0 = f_{sam} - f_{ref}$, and $\Delta Q = Q_{sam} - Q_{ref}$, with the subscript 'sam' for the sample. This system of linear equations is estimated around an arbitrary reference liquid with $\varepsilon_{ref}=\varepsilon'_{ref}+j\varepsilon''_{ref}$, which produces the resonance frequency and Q factor of f_{ref} and Q_{ref}, respectively. The unknown coefficients in the characteristic matrix can be determined from a set of measurements with controlled samples. A benefit from using this empirical model is that fabrication tolerances around the sensing area are fully taken into account.

A binary mixture of distilled water and ethanol at different fractions is chosen to characterize the matrix in Eq. (6), since the dielectric properties of the mixture are well studied in the microwave regime. The volume fraction of water is varied from 0% to 100% with a step size of 10%, giving a dataset of eleven samples. Figure 6 shows the measurement results with the resonance frequency and Q factor as a function of the volume fraction. The resonance frequency is lowered from 1.96 GHz to 1.85 GHz, as the water concentration increases from 0% to 100%. The Q factor is lowest when the water content is around 40% by volume. The corresponding complex permittivity of the mixture can be described by the Debye model as

$$\epsilon_{sam}=\epsilon_{\infty}+\frac{\Delta\epsilon_D}{1-j\omega\tau_D} \quad (7)$$

The high frequency relative permittivity ε_∞, dielectric decrement $\Delta\varepsilon_D$, and Debye relaxation time τ_D are readily available [14]. Figure 7 depicts the complex permittivity of the water-ethanol mixture at around 1.9 GHz obtained by curve fitting to the literature values. The dispersion is not taken into account, since the resonance shift is within a narrow frequency band.

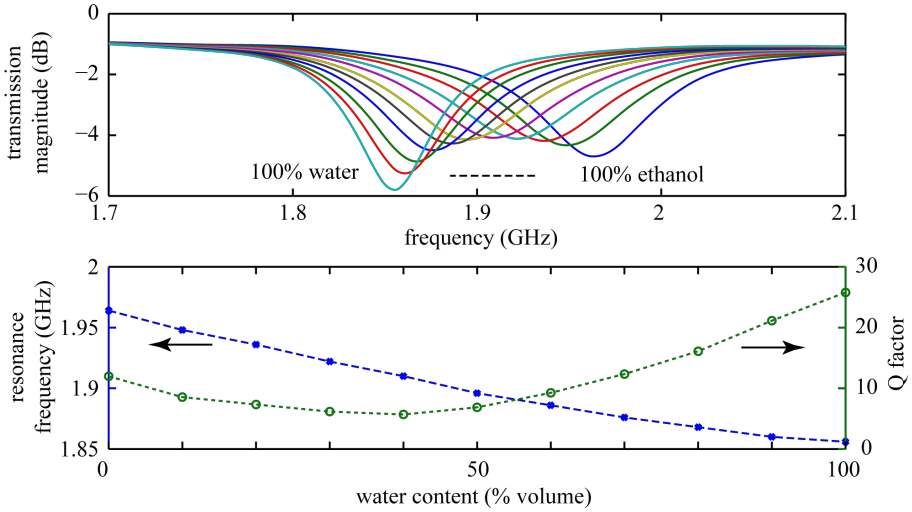

Figure 6. Measured transmission response of water-ethanol mixture at different volume fractions. (a) Transmission magnitude of the mixture when the water content increases from 0% to 100% with a step size of 10% by volume. (b) Corresponding resonance frequency f_0 and Q factor at different steps. The lines are merely for visual guidance.

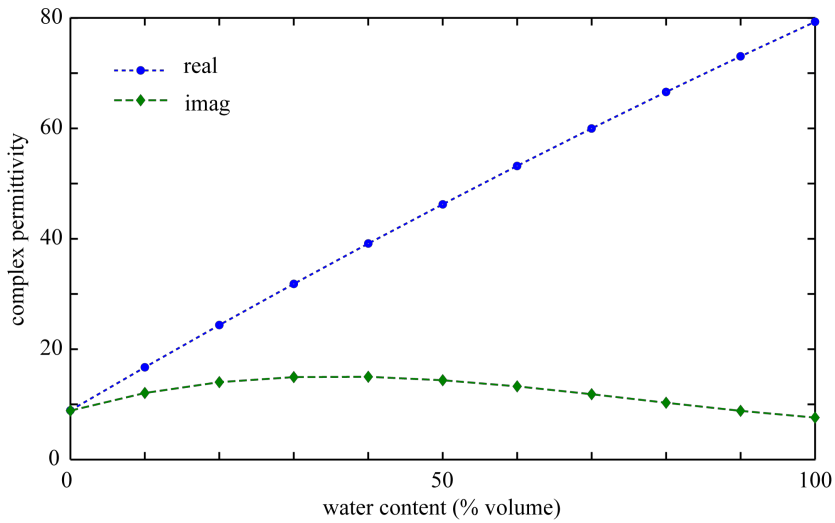

Figure 7. Complex permittivity of water-ethanol mixture. The mixture permittivity at 1.9 GHz is shown as a function of the water content. The values are taken from [14] with polynomial fitting to smooth the curves within the confidence interval.

Since Eq. (6) is overdetermined by the mixture dataset, the method of least squares is used to approximate the unknown coefficients. Three matrices are set up from the reported complex permittivity, measured resonance frequency, and measured Q factor, as

$$X=\begin{bmatrix}\Delta\epsilon'_1 & \Delta\epsilon''_1\\ \Delta\epsilon'_2 & \Delta\epsilon''_2\\ \vdots & \vdots\\ \Delta\epsilon'_{11} & \Delta\epsilon''_{11}\end{bmatrix},\quad Y_1=\begin{bmatrix}\Delta f_1\\ \Delta f_2\\ \vdots\\ \Delta f_{11}\end{bmatrix}\ \text{and}\quad Y_2=\begin{bmatrix}\Delta Q_1\\ \Delta Q_2\\ \vdots\\ \Delta Q_{11}\end{bmatrix}. \quad (8)$$

The indices denote 11 mixtures with a volume fraction of water from 0% to 100%. The mixture at 50% volume fraction is chosen as the reference, from which the elements in these matrices are estimated. The

unknown coefficients can be calculated from

$$[m_{11}\ m_{12}]^T=(X^TX)^{-1}X^TY_1 \text{ and } [m_{21}\ m_{22}]^T=(X^TX)^{-1}X^TY_2 . \quad (9)$$

These equations yield the characteristic matrix that relates the complex permittivity of the liquid under test with the resonance properties as

$$\begin{bmatrix}\Delta f_0\\ \Delta Q\end{bmatrix}=\begin{bmatrix}-0.0016 & -0.0016\\ 0.1111 & -1.9590\end{bmatrix}\begin{bmatrix}\Delta\epsilon'\\ \Delta\epsilon''\end{bmatrix}. \quad (10)$$

The sensor module can be exclusively described by this set of equations, which fully takes into account deviations in the dimensions and properties of constructing materials. Through the matrix inversion, Eq. (10) yields

$$\begin{bmatrix}\Delta\epsilon'\\ \Delta\epsilon''\end{bmatrix}=\begin{bmatrix}-577.33 & 0.46\\ -32.73 & -0.48\end{bmatrix}\begin{bmatrix}\Delta f_0\\ \Delta Q\end{bmatrix}. \quad (11)$$

This empirical model can be used to estimate the unknown complex permittivity of the liquid sample under test from the observed resonance. Section 5 demonstrates a blind test of this model with another water-based mixture.

5. Microfluidic sensing

The resonance-permittivity relation in Eq. (11) is validated in this section. A mixture of water-methanol is chosen as an analyte for microfluidic sensing. Although methanol and ethanol are classified in the same chemical group, their dielectric properties are considerably different. In the pure form, ethanol and methanol have the complex permittivity $\varepsilon'+j\varepsilon''$ of 9+9*j* and 26+13*j*, respectively, at 1.9 GHz. For the water-methanol mixture at different concentrations, the measured transmission response of the sensor is given in Fig. 8, together with the extracted resonance frequency and Q factors. Eq. (11) is then used to resolve the complex permittivity of the mixture from each pair of the resonance frequency and Q factor. Note that the reference values are from the water-ethanol mixture at 50% volume fraction. The results from the microfluidic sensor measurement are plotted against the literature values as a function of the concentration, as shown in Fig. 9. The estimated complex permittivity of the mixture is in reasonable agreement with the literature. Small discrepancies are likely from measurement uncertainties and the first-order approximation of the relation. These inaccuracies can be reduced by using a higher-order approximation of the characteristic model. In addition, a more accurate characteristic matrix can be obtained by testing the sensor with more samples that better cover the solution space (ε', ε'').

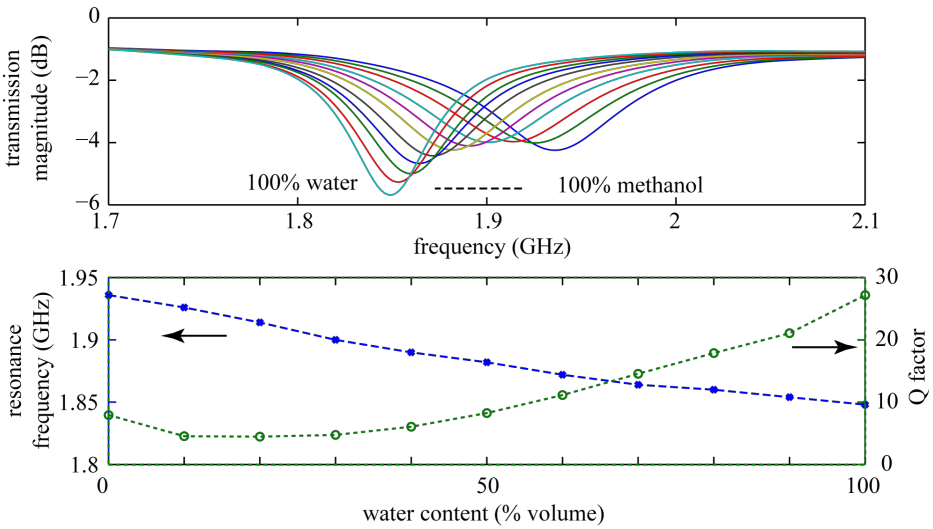

Figure 8 Measured transmission response of water-methanol mixture at different volume fractions. (a) Transmission magnitude of the mixture when the water content increases from 0% to 100% with a step size of 10% by volume. (b) Corresponding resonance frequency f_0 and Q factor at different steps. The lines are merely for visual guidance.

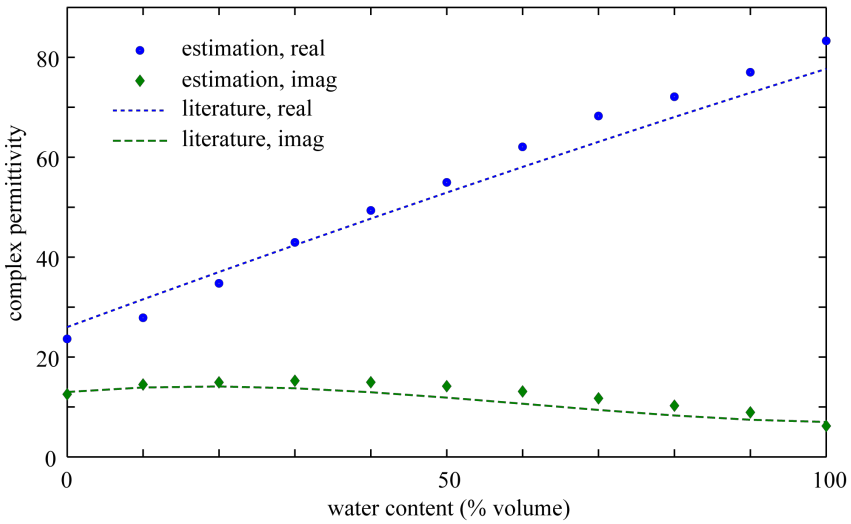

Figure 9. Complex permittivity of water-methanol mixture. The mixture permittivity at 1.9 GHz is shown as a function of the water content. The literature values are taken from [14] with polynomial fitting. The estimated values are derived from the measured resonance in Fig. 8 by using Eq. (11).

6. Conclusion

A high-sensitivity real-time microfluidic sensor based on electromagnetic sensing is demonstrated at microwave frequencies. The main component of the sensor is a SRR, a basic component in metamaterials. Excited by electromagnetic waves, the resonator exhibits strong field confinement in a subdiffraction volume. A small dielectric change in this volume can cause a large change in the resonance frequency. An empirical model can be used to inverse the relation to determine the complex dielectric properties of the sample from the measured frequency and Q-factor of the resonance. In terms of the sample requirement, the cross section of the microfluidic channel can be as small as $(0.001\lambda_0)^2$. The experiments with liquid binary mixtures, including ethanol-water and methanol-water, successfully validate the concept. Owing to its capability of composition quantification and characterization, the proposed sensor and associated technique are very promising for analytical chemistry in a dynamic environment.

Acknowledgements

This research was partially supported by the Australian Research Council Discovery Projects funding scheme under Project DP1095151.

References

[1] W. Withayachumnankul and D. Abbott, “Metamaterials in the terahertz regime,” IEEE Photonics Journal, 1(2), 99-118, 2008.

[2] J. F. O’Hara, R. Singh, I. Brener, E. Smirnova, J. Han, A. J. Taylor, and W. Zhang, “Thin-film sensing with planar terahertz metamaterials: Sensitivity and limitations,” Optics Express, 16(3), 1786-1795, 2008.

[3] W. Withayachumnankul, H. Lin, K. Serita, C. Shah, S. Sriram, M. Bhaskaran, M. Tonouchi, C. Fumeaux, and D. Abbott, “Sub-diffraction thin-film sensing with planar terahertz metamaterials,” Optics Express, 20(3), 3345-3352, 2012.

[4] I. A. I. Al-Naib, C. Jansen, and M. Koch, “Thin-film sensing with planar asymmetric metamaterial resonators,” Applied Physics Letters, 93, 083507, 2008.

[5] W. Withayachumnankul, K. Jaruwongrungsee, C. Fumeaux, and D. Abbott, "Metamaterial-inspired multichannel thin-film sensor," IEEE Sensors Journal, 12(5), 1455-1458, 2012.

[6] B. Reinhard, K. M. Schmitt, V. Wollrab, J. Neu, R. Beigang, and M. Rahm, “Metamaterial near-field sensor for deep-subwavelength thickness measurements and sensitive refractometry in the terahertz

frequency range," Applied Physics Letters, 100(22), 221101, 2012.

[7] H.-J. Lee and J.-G. Yook, "Biosensing using split-ring resonators at microwave regime," Applied Physics Letters, 92(25), 254103, 2008.

[8] H.-J. Lee, J-H. Lee, H.-S. Moon, I.-S. Jang, J.-S. Choi, J.-G. Yook, and H.-I. Jung, "A planar split-ring resonator-based microwave biosensor for label-free detection of biomolecules," Sensors and Actuators B: Chemical, 169, 26-31, 2012.

[9] A. W. Clark, A. Glidle, D. R. S. Cumming, and J. M. Cooper, "Plasmonic split-ring resonators as dichroic nanophotonic DNA biosensors," Journal of the American Chemical Society, 131(48), 17615-17619, 2009.

[10] J. A. Gordon, C. L. Holloway, J. Booth, S. Kim, Y. Wang, J. Baker-Jarvis, and D. R. Novotny, "Fluid interactions with metafilms/metasurfaces for tuning, sensing, and microwave-assisted chemical processes," Physical Review B, 83(20), 205103, 2011.

[11] B. Dong, W. M. Zhu, Y. H. Fu, J. M. Tsai, H. Cai, D. L. Kwong, E. P. Li, E. Rius, A. Q. Liu, "An absorptive filter using microfluidic switchable metamaterials," Solid-State Sensors, Actuators and Microsystems Conference, 530-533, 2011.

[12] N. Wiwatcharagoses, K. Y. Park, J. A. Hejase, L. Williamson, and P. Chahal, "Microwave artificially structured periodic media microfluidic sensor," IEEE Electronic Components and Technology Conference (ECTC), 1889-1893, 2011.

[13] C. L. Holloway. E. F. Kuester, J. A. Gordon, J. O'Hara, J. Booth, and D. R. Smith, "An overview of the theory and applications of metasurfaces: the two-dimensional equivalents of metamaterials," IEEE Antennas and Propagation Magazine, 54(2), 10-35, 2012.

[14] J.-Z. Bao, M. L. Swicord, and C. C. Davis, "Microwave dielectric characterization of binary mixtures of water, methanol, and ethanol," Journal of Chemical Physics, 104(12), 4441-4450, 1996.

Biographies

Withawat Withayachumnankul received the B.Eng. and M.Eng degrees in electronic engineering from King Mongkut's Institute of Technology at Ladkrabang (KMITL), Bangkok, Thailand, in 2001 and 2003, respectively, and the Ph.D. degree in electrical engineering from the University of Adelaide, Adelaide, Australia, in 2010. Currently, he holds an ARC Australian postdoctoral fellowship with the University of Adelaide. His research interests include metamaterials and terahertz technology.

Kata Jaruwongrangsee received the B.Eng. and M.Eng. degrees in electronics engineering from King Mongkut's Institute of Technology Ladkrabang (KMITL), Bangkok, Thailand, in 2003 and 2005, respectively, where he is currently working toward the Ph.D. degree in electronics engineering. Since 2006, he has been with the Nanoelectronics and MEMS Laboratory, National Electronics and Computer Technology Center (NECTEC), Thailand, as an Assistant Researcher. His research is mainly focused on QCM-based sensor technology and its applications.

Adisorn Tuantranont is currently Lab director of Nanoelectronics and MEMS Laboratory, National Electronics and Computer Technology Center (NECTEC), under National Science and Technology Development Agency (NSTDA), Thailand. He received the B.S. degree from King Mongkut's Institute of Technology Ladkrabang (KMITL), Bangkok, Thailand in 1995, and the Ph.D. degree in 2001 from University of Colorado at Boulder, CO, USA, in Electrical Engineering. His current research interests are optical MEMS, microfluidic lab-on-a-chip and optoelectronics packaging.

Christophe Fumeaux received the Diploma and Ph.D. degrees in physics from the ETH Zürich, Switzerland, in 1992 and 1997, respectively. In 2008, he joined the School of Electrical and Electronic Engineering, The University of Adelaide, Adelaide, Australia, as an Associate Professor. Since 2011, he is a Future Fellow of the Australian Research Council. Dr Fumeaux is an Associate Editor for the IEEE

Transactions on Microwave Theory and Techniques. His current main research interest concerns computational electromagnetics, antenna engineering, terahertz technology, and the modeling of optical microstructures/nanostructures.

Derek Abbott received the B.Sc. (Hons) degree in physics from Loughborough University of Technology, Leicestershire, U.K., in 1982, and the Ph.D. degree in electrical and electronic engineering from The University of Adelaide. Since 1987, he has been with The University of Adelaide, where he is presently a full Professor with the School of Electrical and Electronic Engineering. Prof Abbott is a Fellow of the Institute of Physics (IOP), a Fellow of the IEEE, and is currently on the Editorial Boards of the Proceedings of the IEEE, IEEE Photonics, and PLoS ONE.

Highlights

- A technique for microfluidic sensing based on metamaterials is proposed.
- A sensor made from a split-ring resonator provides an exceptional Q factor and field confinement.
- Flowing liquids can be monitored in real-time with minimal amount of sample.
- The dielectric properties of the sample can be extracted from the measurement.
- This sensor suggests a platform for sample identification, classification, and characterization.

List of figure captions

Figure 1. Microstrip-coupled SRR. (a) Diagram (not to scale) of the SRR and microstrip with dimensions as follows: l = 7 mm, w = 7.5 mm, g = 0.15 mm, r = 0.2 mm, c = 0.65 mm, and w_s = 1.7 mm. The metallic structure is supported by a dielectric substrate, which also supports the ground plane on its bottom side. (b) Equivalent circuit with L_m for the inductance of the microstrip line, $\{RLC\}_S$ for the parasitic elements of the ring, and M for the mutual inductance between the ring and line.

Figure 2. Numerically resolved transmission magnitude of the SRR-loaded microstrip. (Inset) Absolute electric field strength over the surface of the structure at 2.1 GHz. The results are for the structure in Fig. 1(a), and are determined with a commercial full-wave electromagnetic solver, CST Microwave Studio, based on the Finite-Integration Technique (FIT).

Figure 3. Assembled sensor module. (a) Fabricated microstrip-coupled SRR with two SMA connectors. The scale is in cm. (b) A zoom-in showing the microfuidic chamber attached to the SRR. The channel with inlet/outlet is laid onto the SRR gap. The arrow indicates the flow direction. (c) Fully assembled module with polymer tubes delivering liquid into the chamber and coaxial cables connected to the vector network analyzer.

Figure 4. Diagram of the experimental setup. The equipment is mainly composed of the vector network analyzer, peristaltic pump, and sensor module. All measurements are performed at room temperature, i.e., around 25 ºC.

Figure 5. Measured transmission response of the sensor module. The profiles represent different measurement conditions: the bare SRR structure without the microfluidic chamber, the assembled sensor with an empty channel, the sensor with channel filled with 100% ethanol, and with 100% water. The Q factor is defined as $f_0/\Delta f$, where Δf is the bandwidth at +3 dB with respect to the minimal transmission.

Figure 6. Measured transmission response of water-ethanol mixture at different volume fractions. (a) Transmission magnitude of the mixture when the water content increases from 0% to 100% with a step size of 10% by volume. (b) Corresponding resonance frequency f_0 and Q factor at different steps. The lines are merely for visual guidance.

Figure 7. Complex permittivity of water-ethanol mixture. The mixture permittivity at 1.9 GHz is shown as a function of the water content. The values are taken from [14] with polynomial fitting to smooth the curves within the confidence interval.

Figure 8 Measured transmission response of water-methanol mixture at different volume fractions. (a) Transmission magnitude of the mixture when the water content increases from 0% to 100% with a step size of 10% by volume. (b) Corresponding resonance frequency f_0 and Q factor at different steps. The lines are merely for visual guidance.

Figure 9. Complex permittivity of water-methanol mixture. The mixture permittivity at 1.9 GHz is shown as a function of the water content. The literature values are taken from [14] with polynomial fitting. The estimated values are derived from the measured resonance in Fig. 8 by using Eq. (11).